Two-Dimensional FTIR Spectroscopy Studies on the Thermal-Oxidative Degradation of Epoxy and Epoxy−Bis(maleimide) Networks

Pellegrino Musto†

Institute of Chemistry and Technology of Polymers, National Research Council of Italy, Via Campi Flegrei, 34, 80078 Pozzuoli (NA), Italy

Received September 13, 2002

ABSTRACT: A recently developed technique, i.e., two-dimensional infrared (2D IR) correlation spectroscopy, has been used to investigate the thermal-oxidative degradation of two networks based on a tetrafunctional epoxy resin. The use of the 2D IR approach to analyze *time-resolved* transmission spectra collected in situ during the high-temperature degradation process effectively enhanced the spectral resolution and revealed details about the reaction mechanism which remain undetected in the one-dimensional, frequency spectra. In particular, the sites of initiation of the auto-oxidative sequence were identified for the case of the plain epoxy resin, as well as the main competitive pathways through which the degradation reaction proceeds. With respect to the network modified by a thermosetting bis(maleimide) comonomer, which displays an IPN-like molecular structure, it was found that the epoxy component undergoes thermal oxidation via the same mechanism as for the plain epoxy network. A limited degradation was detected also for the bis(maleimide) component, whose stability represents the underlying reason for the enhanced temperature performances of the ternary system.

Introduction

Epoxy resins represent one of the most important classes of matrices for structural composites. In particular, the tetraglycidyl-4,4′-diaminodiphenylmethane (TGDDM) cured by aromatic diamines, such as 4,4′-diaminodiphenyl sulfone (DDS) is widely used in adhesives and as encapsulant for electronic components. Furthermore, it is the matrix of choice for high performance carbon-fiber composites in the aerospace industry, owing to its excellent properties in terms of rigidity, T_g, and thermal stability.[1,2] In these particular applications the material is subjected to very rapid temperature jumps (thermal spikes) often exceeding 150 °C, and must be able to sustain these conditions preserving its structural integrity.[3] Clearly, for the TGDDM/DDS system the thermal-oxidative stability is an issue of primary technological concern, and, as such, has stimulated a large body of research aimed at improving this characteristic. A promising approach which has recently emerged consists of the realization of interpenetrating polymer networks (IPNs): in these systems a more stable monomer capable of forming an independent network, is dissolved, before curing, in the TGDDM/DDS mixture.[4−6] Reasonable success has been achieved along this line by use of a thermosetting bis(maleimide) resin [4,4′-bis(maleimido)diphenylmethane (BMI)], as reactive comonomer. With regard to the molecular structure of this system, a detailed spectroscopic analysis has shown that TGDDM and BMI form individual networks without intercross-links between the components. The epoxy resin cross-links through reaction with its hardener, DDS, while BMI polymerizes via a thermally initiated radical process.[7,8] Dynamic mechanical analysis, on the other hand, has revealed a substantial degree of physical interpenetration of the two networks. The presence of the BMI network, which is more "rigid" than that produced by TGDDM has been found to increase such properties as the T_g, the modulus and the yield stress.[7] These improvements have been achieved, however, at the expenses of a slight reduction in fracture toughness, i.e., K_c and G_c.[7,8] The presence of the BMI network in such systems has, furthermore, been found to lower the equilibrium uptake and to increase the diffusivity of water, with respect to the unmodified TGDDM/DDS resin.[8]

With respect to thermal-oxidative stability, a comparative study, performed by thermogravimetry (TGA), dynamic-mechanical analysis and *time-resolved* FTIR spectroscopy has revealed considerable improvements for the BMI modified networks[9] in comparison to the pure TGDDM/DDS resin. In particular, conventional in situ FTIR measurements made it possible to monitor the degradation kinetics of various molecular groups involved in the process, and allowed us to propose likely reaction mechanisms which accounted for the experimental observations.

In the present contribution use is made of a recently developed technique to analyze transient (time-resolved) FTIR spectra, that is, two-dimensional infrared (2D IR) correlation spectroscopy.[10−13] This technique is receiving considerable attention as a powerful tool that can aid in the interpretation of complex spectra, such as those commonly encountered in the infrared spectroscopy of condensed phase systems, which are characterized by broad, multiply overlapped peaks. Among the various advantages provided by 2D IR spectroscopy, the more relevant are the following: (a) the possibility of improving the resolution and of separating highly overlapped peaks; (b) the possibility to provide information about inter- and intramolecular interactions by selective correlation of peaks; (c) the ability of probing the relative rate of spectral intensity changes taking place in the transient process by analysis of the asynchronous cross-correlation spectrum.

2D IR spectroscopy was introduced by Noda[10−12] and was originally intended to be used in conjunction with dynamic rheo-optical data where the perturbation waveform is a simple sinusoid with fixed frequency. More

† E-mail: musto@irtemp.na.cnr.it.

10.1021/ma0214815 CCC: $25.00
Published on Web 04/02/2003

recently, the same author[13] has further extended the underlying theory by introducing a more general formalism to include dynamic IR signals having any arbitrary waveform. In this work it is shown that the 2D IR correlation analysis of the transient spectra obtained during an isothermal degradation process provide a mean for effectively enhancing the spectral resolution and for highlighting subtle effects that remain undetectable in the conventional one-dimensional analysis.

Theory

In this section the aspects of the theory of 2D IR correlation spectroscopy relevant to the application of this technique to problems of chemical kinetics are reviewed in some details in order to highlight the meaning of the cross-correlation spectra for the specific case of exponential decay functions.

The basic scheme used in 2D IR spectroscopy consists of applying an external perturbation with fixed waveform and analyzing the dynamic response of the system in the form of spectroscopic signals.[10−12] Typical spectroscopic responses to external stimuli are observed in the form of changes in peak positions, intensities and directional absorbances (dichroic effects). In its original formulation 2D IR analysis was developed for the specific case of a sinusoidally varying perturbation for which a relatively simple analytical solution is available.[10−12] However, it was soon recognized that the particular excitation waveform does not alter the basic principles of 2D IR analysis, and more recently, Noda[13] introduced a generalized formalism which can be applied, in principle, to any excitation waveform. With this new formalism, the applicability range of the two-dimensional correlation approach has been greatly extended.[14−22]

Considering a time-dependent spectral intensity $y(\nu,t)$ observed for a period between $-T/2$ and $T/2$, the *dynamic spectrum* $\tilde{y}(\nu,t)$ is defined as

$$\tilde{y}(\nu,t) = \begin{cases} y(\nu,t) - \bar{y}(\nu) & \text{for } -T/2 \le t \le T/2 \\ 0 & \text{otherwise} \end{cases} \quad (1)$$

$\bar{y}(\nu)$is the *reference spectrum* and can be selected in a number of ways depending on the specific excitation waveform.[14−16] In dealing with nonperiodic time-dependent behavior, as in the present case, the most effective choice of the *reference spectrum* is the *ground-state spectrum* of the system, well before the application of the excitation ($t \rightarrow -\infty$).[15,16]

The complex cross-correlation intensity between dynamic spectral intensities at wavenumbers ν_1 and ν_2 is defined as

$$\Phi(\nu_1,\nu_2) + i\Psi(\nu_1,\nu_2) = \frac{1}{\pi T}\int_0^\infty \tilde{Y}(\nu_1,\omega)\ \tilde{Y}^*(\nu_2,\omega)\ \mathrm{d}\omega \quad (2)$$

In the above equation, $\tilde{Y}(\nu_1,\omega)$ represents the forward Fourier transform (FT) of the dynamic spectral intensity $\tilde{y}(\nu_1,t)$, i.e.

$$\tilde{Y}(\nu_1,\omega) = \int_{-\infty}^{\infty} \tilde{y}(\nu_1,t)\mathrm{e}^{-i\omega t}\,\mathrm{d}t \quad (3)$$

while $\tilde{Y}^*(\nu_2,\omega)$ is the conjugate of the FT of the dynamic spectral intensity $\tilde{y}(\nu_2,t)$, that is

$$\tilde{Y}^*(\nu_2,\omega) = \int_{-\infty}^{\infty} \tilde{y}(\nu_2,t)\mathrm{e}^{i\omega t}\,\mathrm{d}t \quad (4)$$

From eq 4, the *synchronous* and *asynchronous* correlation intensities can be explicitly written in terms of the real and imaginary components of the FT as

$$\Phi(\nu_1,\nu_2) = \frac{1}{\pi T}\int_0^\infty \{\mathrm{Re}[\tilde{Y}(\nu_1,\omega)]\ \mathrm{Re}[\tilde{Y}(\nu_2,\omega)] + \mathrm{Im}[\tilde{Y}(\nu_1,\omega)]\ \mathrm{Im}[\tilde{Y}(\nu_2,\omega)]\}\ \mathrm{d}\omega \quad (5)$$

$$\Psi(\nu_1,\nu_2) = \frac{1}{\pi T}\int_0^\infty \{\mathrm{Im}[\tilde{Y}(\nu_1,\omega)]\ \mathrm{Re}[\tilde{Y}(\nu_2,\omega)] - \mathrm{Re}[\tilde{Y}(\nu_1,\omega)]\ \mathrm{Im}[\tilde{Y}(\nu_2,\omega)]\}\ \mathrm{d}\omega \quad (6)$$

Equations 5 and 6 are often employed for the numerical evaluation of the functions $\Phi(\nu_1,\nu_2)$ and $\Psi(\nu_1,\nu_2)$ by direct Fourier transformation of the experimental spectra.[23] Recently, a more efficient approach based on the Hilbert transform has been proposed,[24] which is the one adopted in the present contribution (see Experimental Section).

If we consider the specific case of time-dependent spectral intensities having an exponential decay dynamic behavior, the general form of such intensity at wavenumber ν can be expressed as

$$y(\nu,t) = \begin{cases} \tilde{y}(\nu,t) = A(\nu)\mathrm{e}^{-k(\nu)t} & \text{for } t \ge 0 \\ 0 & \text{otherwise} \end{cases} \quad (7)$$

where $A(\nu)$ and $k(\nu)$ are the coefficient of the decay process and the characteristic rate constant, respectively. To determine the complex cross-correlation function, we consider two spectral intensities at frequencies ν_1 and ν_2, having different values of A and k. The Fourier transform, $\tilde{Y}(\nu_1,\omega)$ and the complex conjugate Fourier transform, $\tilde{Y}^*(\nu_2,\omega)$ of these dynamic spectral intensities are given by

$$\tilde{Y}(\nu_1,\omega) = \int_0^\infty A(\nu_1)\mathrm{e}^{-k(\nu_1)t}\mathrm{e}^{-i\omega t}\,\mathrm{d}t = \frac{A(\nu_1)}{k(\nu_1) + i\omega} \quad (8)$$

$$\tilde{Y}^*(\nu_2,\omega) = \int_0^\infty \mathrm{e}^{-k(\nu_2)t}\mathrm{e}^{-i\omega t}\,\mathrm{d}t = \frac{A(\nu_2)}{k(\nu_2) - i\omega} \quad (9)$$

Thus, eq 2 becomes

$$\Phi(\nu_1,\nu_2) + i\Psi(\nu_1,\nu_2) = \frac{A(\nu_1)A(\nu_2)}{\pi T}\int_0^\infty \frac{k(\nu_1)k(\nu_2) + i[k(\nu_1) - k(\nu_2)]\omega + \omega^2}{[k^2(\nu_1) + \omega^2][k^2(\nu_2) + \omega^2]}\,\mathrm{d}\omega \quad (10)$$

from which the synchronous and asynchronous correlation intensities can be evaluated by solving the integral in the left side of eq 10:[16]

$$\Phi(\nu_1,\nu_2) = \frac{A(\nu_1)A(\nu_2)}{T}\frac{1}{k(\nu_1) + k(\nu_2)} \quad (11)$$

$$\Psi(\nu_1,\nu_2) = \frac{A(\nu_1)A(\nu_2)}{\pi T}\frac{\ln k(\nu_2) - \ln k(\nu_1)}{k(\nu_1) + k(\nu_2)} \quad (12)$$

Equations 11 and 12 highlight the meaning of the synchronous and asynchronous spectra. In the synchronous spectrum a peak will appear at coordinates (ν_1,ν_2) whenever there is a pair of peaks located at ν_1 and ν_2 in the frequency spectrum undergoing simultaneous intensity changes during the sampling interval. The

synchronous spectrum is symmetric [i.e. $\Phi(\nu_1,\nu_2) = \Phi(\nu_2,\nu_1)$] and consists of *autopeaks* located along the main diagonal (i.e at coordinates ν_i, ν_i) and *cross-peaks* appearing at off-diagonal positions. The autopeaks identify the signals that undergo changes during the experiment. They are always positive and their intensity can be considered as a measure of the susceptibility of the relative signals to the external stimulus.[14,15] The cross-peaks, on the other hand, are positive if the two signals change in the same direction (they both increase or decrease) and are negative otherwise.

The asynchronous correlation spectrum identifies decay processes having different rates as a result of the term $\ln k(\nu_2) - \ln k(\nu_1)$, which assume nonzero values only if the rate constants for the decay processes at the two wavenumbers are different. Therefore, it contains no autopeaks but only cross-peaks at off-diagonal positions. The asynchronous spectrum is antisymmetric [i.e. $\psi(\nu_1,\nu_2) = -\psi(\nu_2,\nu_1)$]; a cross-peak at coordinates (ν_1,ν_2) is positive if the intensity change at ν_1 is accelerated with respect to that at ν_2 and is negative otherwise. However, this rule is reversed if $\Phi(\nu_1,\nu_2) < 0$.[14−16] A direct comparison between the synchronous and asynchronous spectra is also informative. Recalling that any two intensities changing simultaneously with time will produce synchronous peaks while only those changing at different rates will give rise to asynchronous peaks, a synchronous peak at (ν_1,ν_2) having no counterpart in the asynchronous spectrum, indicates that the decay processes at the corresponding frequencies are occurring at the same rate.

Experimental Section

Materials and Preparation Procedures. The epoxy monomer was a commercial grade of tetraglycidyl-4,4′diaminodiphenylmethane (TGDDM), supplied by Ciba-Geigy (Basel, Switzerland). It had an epoxy equivalent weight (EEW) of 124.1 g equiv^{-1}, measured by potentiometric titration. The hardener was 4,4′-diaminodiphenyl sulfone (DDS), received from Aldrich (Milwaukee, WI) and the bis(maleimide) component was *N*,*N*′-bis(maleimide)-4,4′-diphenylmethane (BMI), also from Aldrich. The reagents were used as received, without further purification. Details about the preparation procedures for the TGDDM/DDS resin and the ternary TGDDM/DDS/BMI mixtures are reported elsewhere.[7,8] The composition of the reactive mixtures was 100/30 weight ratio (corresponding to 1/0.5 mol ratio) for the TGDDM/DDS network, and 100/30/100 weight ratio (corresponding to 1/0.5/1.2 mol ratio) for the TGDDM/DDS/BMI network.

To obtain infrared spectra suitable for quantitative analysis according to the Beer−Lambert relationship, the absorbance of the peaks of interest must not exceed values in the region 1.3−1.5 units. Films for these studies (5−10 μm of thickness) were prepared by dissolving TGDDM, DDS, and BMI in the appropriate amounts, in acetone (total concentration 10 wt %), followed by casting on KBr disks and vacuum-drying. Curing (140°C, 16 h) and post-curing (200°C, 4 h) were carried out under nitrogen.

FTIR Spectroscopy. Transmission FTIR spectra were obtained using a System 2000 spectrometer from Perkin-Elmer (Norwalk, CT). This instrument employs a germanium/KBr beam splitter and a deuterated tryglycine sulfate (DTGS) detector. The instrumental parameters adopted for the spectral collection were as follows: resolution 4 cm^{-1}, optical path difference (OPD) velocity = 0.20 cm s^{-1}, and spectral range 4000−400 cm^{-1}. A single data collection was performed for each spectrum (3551 data points) which, in the selected instrumental conditions took 6 s to complete. It was found that, even with a single acquisition, the signal-to-noise ratio of the spectra (5000:1) was suitable for 2D IR analysis. A typical kinetic test comprised 200 spectra acquired at intervals of 5 min over a time period of 1000 min. A dedicated software package for the acquisition of time-resolved infrared spectra was used to drive the FTIR spectrometer during the test (Timebase V. 1.1 from Perkin-Elmer).

The isothermal kinetic measurements of the degradation process were carried out in an environmental chamber directly fitted in the spectrometer, which was constructed in house by modifying the commercially available SPECAC 20100 cell. This unit was controlled by a Eurotherm PID temperature regulator model 2416, with an accuracy of ±0.5 °C. All measurement were carried out at 200 °C under a continuous flux of air (60 cm^3 min^{-1}).

2D IR Correlation Analysis. Before performing cross-correlation analysis, the experimental spectra were preprocessed to avoid the occurrence of artifacts due to baseline instabilities and other nonselective effects.[25,26] The frequency regions of interest (2600−3800 and 1400−1950 cm^{-1}) were truncated and were subjected to a linear baseline correction, followed by offset to the zero absorbance value. Generalized 2D IR analysis was performed by a computer program composed by the author within the Grams/32 environment (Galactic Industries Co., Salem, NH), using the associated programming language Array Basic.

A recently developed algorithm was employed, which does not rely directly on Fourier transformation but rather on the Hilbert transform, and offers an easier and more efficient method for the numerical evaluation of the correlation intensities.[24] In matrix notation, a discrete set of dynamic spectra measured at m equally spaced time intervals between T_{min} and T_{max} may be conveniently expressed as a column vector:

$$\tilde{\mathbf{y}}(\nu) = \begin{bmatrix} \tilde{y}(\nu,t_1) \\ \tilde{y}(\nu,t_2) \\ \dots \\ \tilde{y}(\nu,t_m) \end{bmatrix} \tag{13}$$

With this notation, the synchronous and asynchronous spectra are concisely represented as

$$\mathbf{\Phi}(\nu_1,\nu_2) = \frac{1}{m-1}\,\tilde{\mathbf{y}}(\nu_1)^{\mathrm{T}}\tilde{\mathbf{y}}(\nu_2) \tag{14}$$

$$\mathbf{\Psi}(\nu_1,\nu_2) = \frac{1}{m-1}\,\tilde{\mathbf{y}}(\nu_1)^{\mathrm{T}}\mathbf{N}\tilde{\mathbf{y}}(\nu_2) \tag{15}$$

where **N** is the Hilbert−Noda transformation matrix, given by

$$N_{jk} = \begin{cases} 0 & \text{if } j = k \\ \dfrac{1}{\pi(k-j)} & \text{otherwise} \end{cases} \tag{16}$$

Equations 14 and 15 constitute the algorithms embodied in the program for the calculation of the 2D IR spectra. The 2D correlation analysis was performed on an evenly spaced sequence of 50 spectra collected with a constant sampling interval of 20 min. It was found that considering shorter time intervals does not improve the quality and resolution of the resulting correlation spectra.

The notation adopted to identify the peaks appearing in the correlation spectra is the following: the *x*-axis frequency coordinate is written first, followed by the *y*-axis coordinate, both enclosed in square brackets. Following the coordinate values, a ± sign enclosed in round brackets specifies the positive or negative value of the peak. The sign is omitted for autopeaks, as these are always positive. It is explicitly noted that, to be concise, only the peaks appearing in the lower side of the spectrum with respect to the diagonal line with coordinates $[\nu_i,\nu_i]$ are referred to, with the understanding that, due to the symmetry of the correlation spectra, corresponding cross-peaks are located in the upper side of the spectrum, at appropriate positions. Also, whenever the number of peaks is mentioned, it is referred to those appearing in the lower side

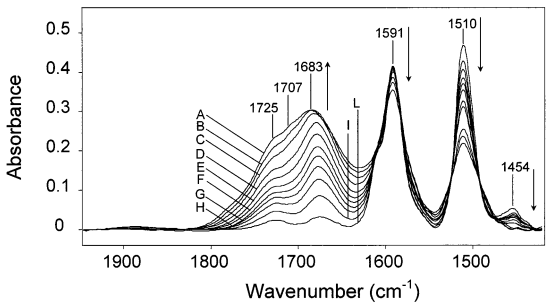

Figure 1. Transmission FTIR spectra in the wavenumber range 1950−1400 of the TGDDM/DDS network collected in situ at different times during thermal-oxidative degradation. Traces: (A) collection time, t, = 0 min; (B) t = 25 min; (C) t = 50 min; (D) t = 75 min; (E) t = 125 min; (F) t = 250 min; (G) t = 350 min; (H) t = 500 min; (I) t = 750 min; (L) t = 1000 min. Arrows' direction indicates absorbance increase or decrease of the corresponding peaks.

of the correlation spectrum, with the understanding that the total number of peaks is twice the reported value.

Results and Discussion

Unmodified Epoxy Network (TGDDM/DDS System). Carbonyl Range (2000—1400 cm^{-1}). In the present contribution the attention is focused on the two regions of the infrared spectrum that are more sensitive to the molecular rearrangements taking place during the thermal-oxidative process. These regions occur between 1950 and 1400 and between 3800 and 2600 cm^{-1}. Figure 1 depicts a series of transmission FTIR spectra in the 1950−1400 cm^{-1} interval, collected at various times for the TGDDM/DDS epoxy system during the degradation process. Extensive changes are apparent, and in particular, the steady increase of a multicomponent carbonyl band, and the decrease of two aromatic absorptions at 1591 and 1510 cm^{-1} and of a low intensity peak at 1454 cm^{-1}.

The synchronous cross-correlation spectrum obtained from the data of Figure 1 is displayed in the form of a pseudo three-dimensional plot (i.e., a fish-net representation) in Figure 2. Underneath the intensity surface, it is also shown the contour plot obtained therefrom. In this alternative representation, the peaks can be quickly identified as the spots of brighter (positive) or darker (negative) color with respect to the uniform color of the background. The contour plot gives only a qualitative account of the features present in the correlation spectra. The evaluation of the exact coordinates of the various peaks and of their true intensity requires examination of the whole intensity surface by appropriate software tools, followed by analysis of several slice diagrams cut along one of the two frequency coordinates. Nevertheless, it appears that contour plots remain the more efficient way to give, in a single, static view, an overall representation of the correlation spectra, and therefore, is the type of representation adopted in the rest of the present contribution.

In the synchronous spectrum displayed in Figure 2 only two autopeaks are evident at [1683, 1683 cm^{-1}] and at [1510, 1510 cm^{-1}], corresponding to the spectral features that are more sensitive to thermal oxidation. The peaks at 1591 and 1454 cm^{-1} produce only a very limited autocorrelation intensity, owing to a more limited variation and, therefore, do not display themselves as autopeaks. However, at least the peak at 1454 cm^{-1} gives rise to distinct cross-peaks.

Unlike the autopeak at [1510, 1510 cm^{-1}] which is very sharp, the one centered at [1683, 1683 cm^{-1}] is considerably broader, reflecting the unresolved, multicomponent profile of the carbonyl band from which it originates. Three distinct cross-peaks are identified at [1683, 1510 cm^{-1} (−)], [1683, 1454 cm^{-1} (−)] and [1510, 1454 cm^{-1} (+)], corresponding to the simultaneous change of the associated functional groups. It is noted that the cross-peaks involving the 1683 cm^{-1} band display a characteristic elongated shape as a consequence of the convolution between a broad band and a sharp peak. The two above cross-peaks are both negative, reflecting the fact that the spectral features from which they derive, change in the opposite direction.

In Figure 3 is reported the asynchronous correlation spectrum calculated from the data of Figure 1, which clearly evidence the resolution enhancement obtained by spreading the spectrum over the second frequency dimension. In the carbonyl area, two distinct features are found, centered, respectively, at [1710, 1676 cm^{-1} (−)] and [1676, 1641 cm^{-1} (+)]. This indicates that the 1676 cm^{-1} component, which forms the main contribution in the carbonyl profile, increases at a faster rate than the species absorbing above 1700 cm^{-1}. These latter species absorb in a relatively wide range of frequencies, as indicated by the elongated shape of the relative cross-peak, but the most intense component occurs at 1710 cm^{-1}, in correspondence to the maximum of the cross-peak.

In a previous contribution,[9] a thermal-oxidative degradation mechanism was proposed on the basis of time-resolved FTIR spectroscopy results, which identified several concurrent pathways. One of these routes produces amide species (structure **I**) while another route gives rise to the ketonic structure **II** and to the unsaturated aldehyde species **III**.

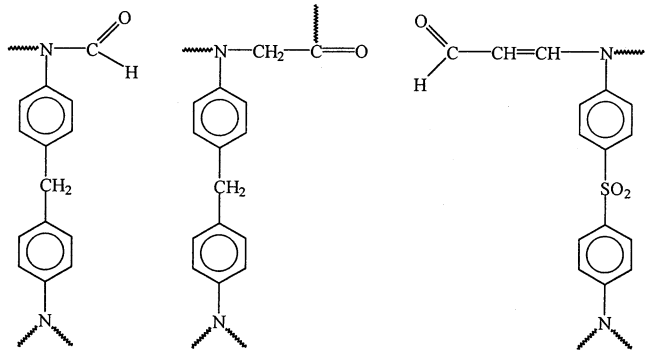

The 1676 cm^{-1} component may safely be identified with the amide group **I**, while the functional groups absorbing above 1700 cm^{-1} arise from the aldehyde and ketone groups **III** and **II**. The wide absorption range is likely related to the multiplicity of species formed and/or to the occurrence of molecular interactions of the hydrogen bonding type, which lower the frequency of the carbonyl stretching absorption. In particular, the principal component at 1710 cm^{-1} may originate from $\alpha-\beta$ unsaturated aldehydes (**III**) and/or to the ketonic groups **II** interacting with proton donor moieties such as −OH and −NH, localized onto the network. The mechanisms giving rise to amide groups and to aldehyde/ketone structures are competitive and the results

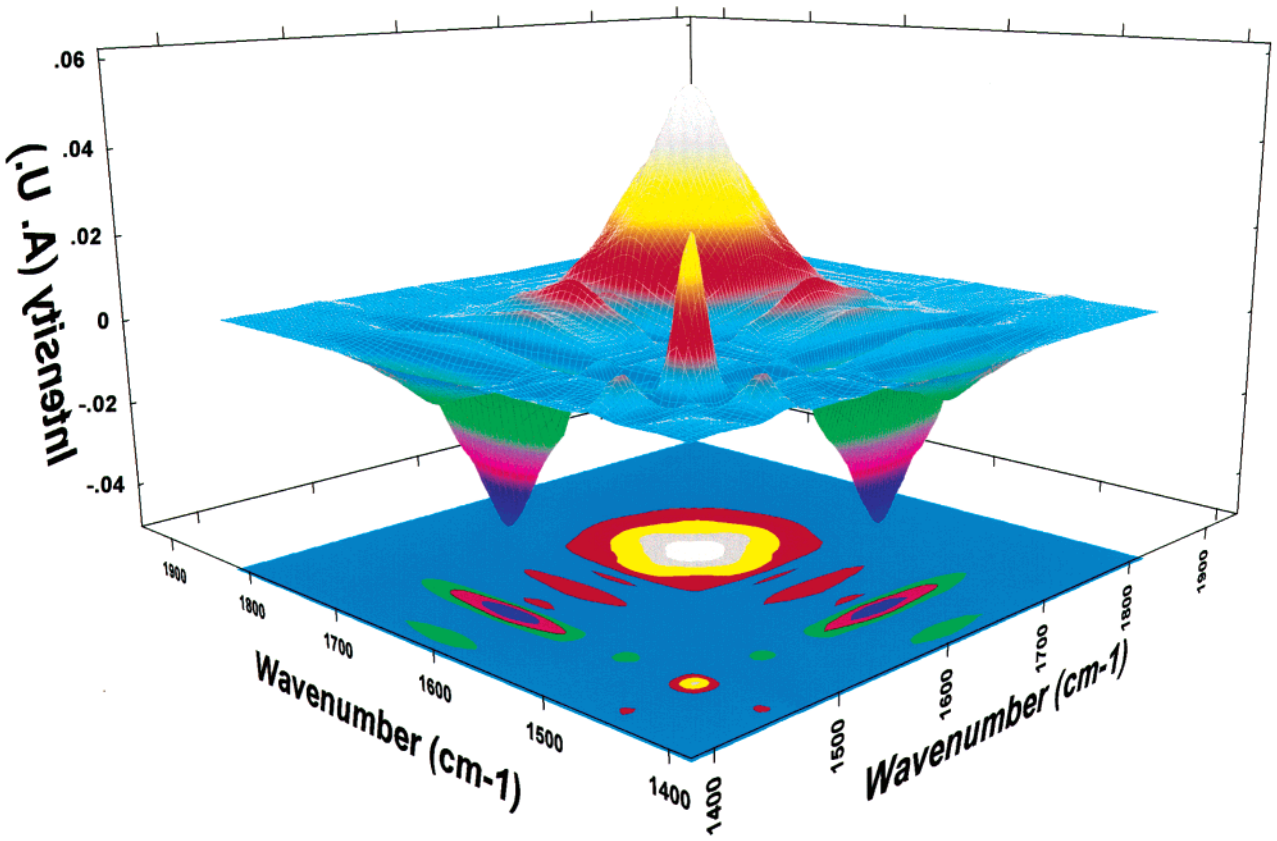

Figure 2. Three-dimensional plot of the synchronous 2D correlation spectrum (fish-net representation) in the wavenumber range 1450−1900 cm^{-1} for the TGDDM/DDS network. Below the three-dimensional diagram, is represented the contour plot obtained from the intensity surface.

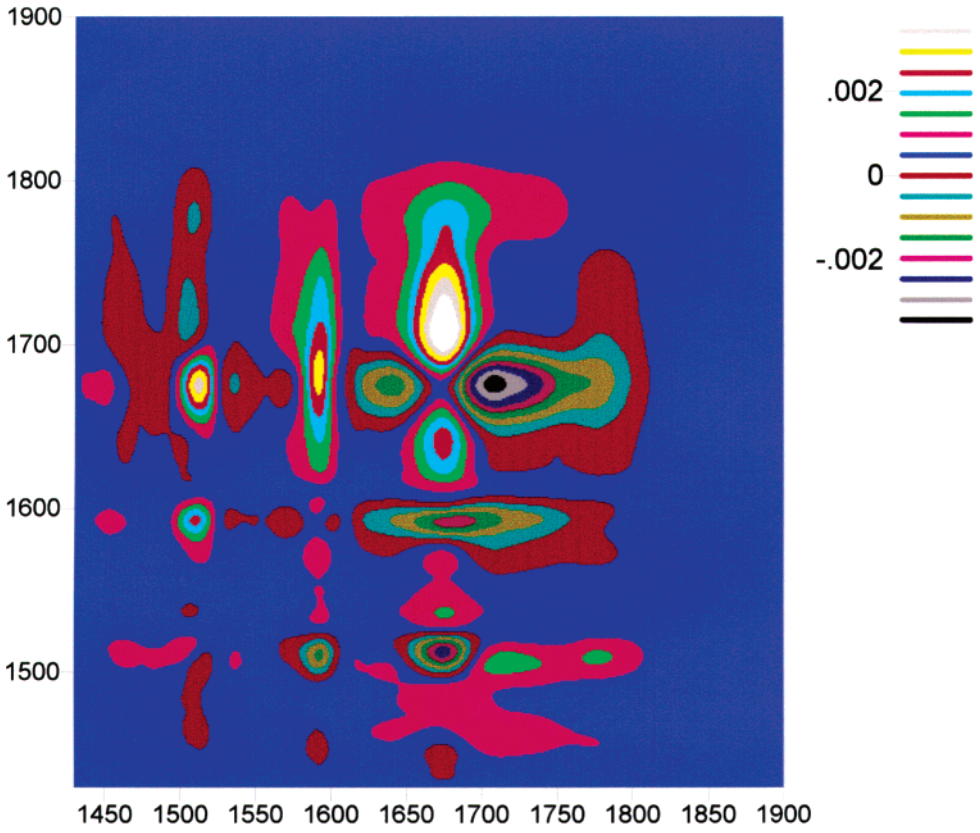

Figure 3. Asynchronous 2D correlation spectrum in the wavenumber range 1450 −1900 cm^{-1} for the TGDDM/DDS network.

of the 2D IR analysis point to the predominance of the former pathway.

With respect to the species at 1641 cm^{-1} identified as a cross-peak in the asynchronous spectrum, it is

likely to be attributed to amide linkages interacting with the proton donor groups (−OH, −NH) of the network. The amide linkages, once formed, have to find the appropriate group to form the molecular interaction, and this accounts for the temporal relationship evidenced in the asynchronous peak (the 1676 cm^{-1} component increasing at a faster rate than the one at 1641 cm^{-1}).

The 1676 cm^{-1} component produces two other cross-peaks arising from the correlation with the two aromatic peaks at 1591 and 1510 cm^{-1}. We recall that, according to the assignments proposed in ref 9, the 1591 cm^{-1} peak is due to a ring stretching mode of the p-disubstituted aromatic ring of the DDS unit, while the 1510 cm^{-1} peak originates from a ring stretching mode of the TGDDM aromatics:

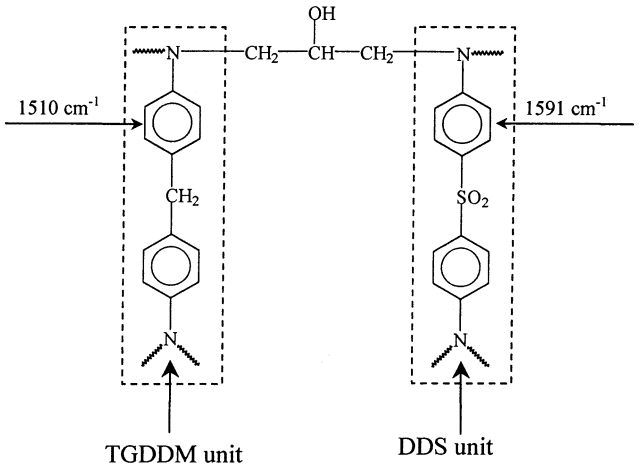

The signs of the asynchronous peaks indicate that the amide carbonyl changes at a faster rate than the two aromatic peaks [Ψ(1676, 1591) and Ψ(1676, 1510) < 0; Φ(1676, 1591 cm^{-1}) and Φ(1676, 1510 cm^{-1}) < 0]. According to the degradation mechanisms proposed in ref 9, the loss of aromatic rings is mainly related to the mechanisms producing aldehyde and ketone groups, while the amide groups originate from an alternative route mainly involving the aliphatic moiety of the network. Therefore, the temporal relationships deduced from the above cross-peaks confirm the conclusions already anticipated from the analysis of the carbonyl area, i.e., that the "amide route" prevails over the "aldehyde/ketone route".

A further relevant feature to be discussed is the asynchronous peak relating the two aromatic rings of the TGDDM and DDS units, which is found at [1512, 1592 cm^{-1} (−)]. The sign of the peak indicates that the concentration of TGDDM aromatic rings decreases at a faster rate than that of the DDS aromatics. This conclusion is in agreement with an earlier kinetic analysis of the degradation process made by conventional, time-resolved FTIR spectroscopy[9] and can be accounted for by assuming the occurrence of an independent degradation pathway starting at the methylene groups joining two aromatic rings in the TGDDM unit. Clearly, this additional mechanism will involve selectively the TGDDM aromatics, since the DDS unit has a much more stable substituent in this position (SO_2 group).

2D IR analysis provides further evidence for the direct involvement of the methylene groups in the degradation mechanism. In fact a composite peak characteristic of the various CH_2 groups can be identified at 1454 cm^{-1}

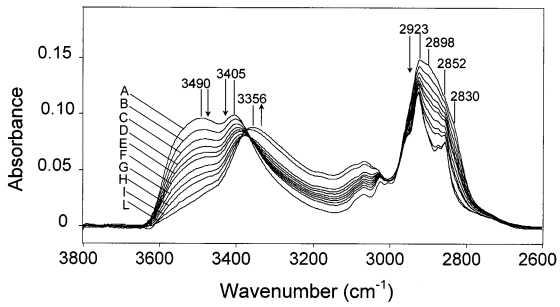

Figure 4. Transmission FTIR spectra in the wavenumber range 3800−2600 of the TGDDM/DDS network collected in situ at different times during thermal-oxidative degradation. Traces: (A) collection time, t, = 0 min; (B) t = 25 min; (C) t = 50 min; (D) t = 75 min; (E) t = 125 min; (F) t = 250 min; (G) t = 350 min; (H) t = 500 min; (I) t = 750 min; (L) t = 1000 min. The arrows' directions indicate absorbance increase or decrease of the corresponding peaks.

(an in-plane deformation mode). This feature is found to decrease with time (see Figure 1) and to produce two distinct cross-peaks in the synchronous spectrum (see Figure 2) relating this signal with the carbonyl absorption [1683, 1545 cm^{-1} (−)] and with the TGDDM aromatic peak [1510, 1454 cm^{-1} (+)].

2600—3800 cm^{-1} Range. In Figure 4 are reported several FTIR spectra in the 3800−2600 cm^{-1} interval, collected at various times for the TGDDM/DDS epoxy system during the degradation process. It is noted that the broad band originally centered at about 3500 cm^{-1}, due to extensively self-associated O−H groups, decreases considerably and shifts at 3356 cm^{-1}, indicating the formation of new species absorbing in the lower side of the ν_{OH} range. In the ν_{CH} range, a complex and unresolved multiplet is observed, originally centered at 2923 cm^{-1}, which decreases in intensity and changes substantially in shape. Clearly, the resolution enhancement brought about by 2D IR analysis is particularly useful in this frequency range to unravel details which remain undetectable in the mono-dimensional spectra.

Figure 5 depicts the synchronous spectrum in the 2600−3800 cm^{-1} range, which exhibits three distinct autocorrelation peaks centered, respectively, at [2834, 2834 cm^{-1}], [2890, 2890 cm^{-1}], and [3512, 3512 cm^{-1}]. Those located below 3000 cm^{-1} are very sharp, while the one at higher frequency gives rise to a broad area reflecting, as in the carbonyl range, the wide shape of the band from which it originates. The three autopeaks give rise to three corresponding cross-peaks at [2890, 2834 cm^{-1} (+)], [2834, 3512 cm^{-1} (+)] and [2890, 3512 cm^{-1} (+)] which are all positive, since the spectral features they derive from, simultaneously decrease with time. The new component appearing at 3356 cm^{-1} (see Figure 4) does not produce an autopeak, since it originates from a gradual shift of the feature initially centered at 3405 cm^{-1}. However, it produces three characteristic cross-peaks having the flat and elongated shape typical of cross-correlation intensities deriving from peak shifts.[25,26]

The asynchronous spectrum is shown in Figure 6, parts A and B. As in the case of the carbonyl region, it displays the maximum enhancement of spectral resolution and the maximum amount of details. This effect is to be related to the enhanced selectivity of the asynchronous cross-correlation function, which, in turn, derives from the term $\ln k(\nu_2) - \ln k(\nu_1)$ (see eq 13).

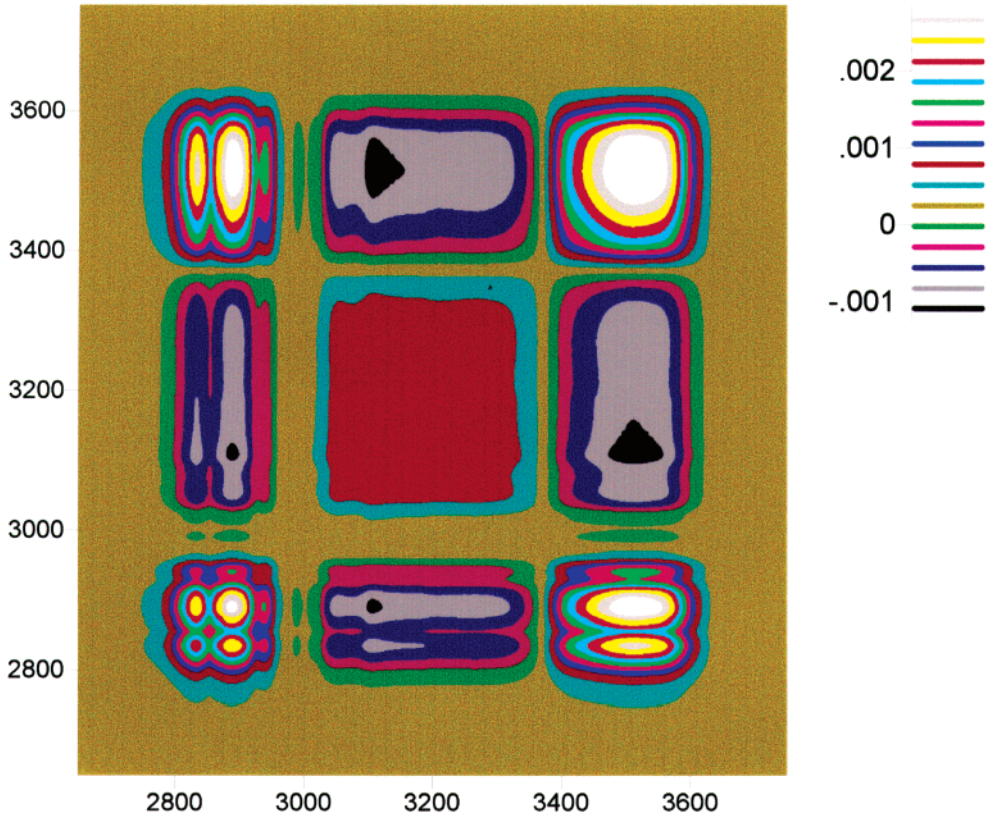

Figure 5. Synchronous 2D correlation spectrum in the wavenumber range 2700−3800 cm^{-1} for the TGDDM/DDS network.

The region below 3000 cm^{-1} (see Figure 6B) is characterized by five sharp peaks, located, respectively, at [2926, 2835 cm^{-1} (+)], [2926, 2884 cm^{-1} (+)], [2958, 2835 cm^{-1} (+)], [2958, 2884 cm^{-1} (+)], and [2943, 2926 cm^{-1} (−)]. Of the five components from which the asynchronous peaks originate, the one at 2884 cm^{-1} can be unambiguously identified as the ν_{CH} vibration of the tertiary carbon atom (R_2−CH−OH group). Analogously, the components at 2958, 2943, and 2926 cm^{-1} can be associated with the out-of-phase stretching vibrations (ν_{as}) of different methylene groups. In particular, the 2958 cm^{-1} peak is seen to increase in intensity during the later stages of the process and therefore is to be associated with a CH_2 group being formed as a consequence of molecular rearrangements. In view of the rather high absorption frequency, it is tentatively assigned to the methylene linked to the nitrogen atom and to the carbonyl group in the ketonic structure **II**. The 2943 and the 2926 cm^{-1} components both decrease steadily with time and can be attributed to the two different CH_2 groups present in the TGDDM/DDS network, i.e., those located on the aliphatic portion of network, next to the nitrogen atoms, and those connecting the aromatic rings of the TGDDM unit. In view of the fact that CH_2 groups linked to −NHR or $-NR_2$ groups absorb at frequencies slightly higher than the usual interval,[27−29] we tentatively assign the component at 2943 cm^{-1} to the latter species. Finally, the remaining feature at 2835 cm^{-1} is likely to be associated with a CH_2 symmetric stretching, possibly corresponding to the ν_{as} vibration at 2943 cm^{-1}, since no cross-peaks are observed at the relative frequency coordinates, as expected for two peaks sharing exactly the same rate of change.

The results of the 2D IR analysis confirm the involvement of the aliphatic portion of the TGDDM/DDS network both at the tertiary carbon atom and at the methylene positions. The direct involvement of the CH_2 group linked to the aromatic rings of the TGDDM unit is further substantiated. The positive value of the asynchronous intensities at [2926, 2835 cm^{-1}] and [2926, 2884 cm^{-1}], taken together with the negative value of the peak at [2943, 2926 cm^{-1}] indicate that the degradation mechanism initiating at the CH_2 position within the TGDDM unit is faster than that starting onto the aliphatic unit, i.e., that the aromatic disubstituted methylene is the less stable.

Above 3000 cm^{-1} a wide, unresolved area is observed, with minima at [3550, 3315 cm^{-1} (−)] and [3550, 3115 cm^{-1} (−)]. These features are related to the decrease of the broad band due to due to extensively hydrogen-bonded O−H groups, coupled with the shift of its maximum toward lower frequencies. The decrease of the ν_{OH} absorption also produces a series of cross-peaks in connection with the already discussed components in the ν_{CH} frequency range. In particular, distinct minima are revealed at [3550, 2958 cm^{-1} (−)], [3550, 2926 cm^{-1} (−)] and a maximum at [3550, 2880 cm^{-1} (+)]. The temporal relationship deduced from the sign of the [3550, 2926 cm^{-1}] peak points to a faster rate of consumption of CH_2 with respect to hydroxyl groups. It has been proposed[9] that the auto-oxidation sequence in TGDDM/DDS networks starts by dehydration followed by hydrogen abstraction at the allylic position. The previous result seems to indicate a concurrent initiation directly onto the methylene group.

Ternary System TGDDM/DDS/BMI. Carbonyl Range (2000—1400 cm^{-1}). Figure 7 displays a series of spectra in the 2000−1420 cm^{-1} interval, collected at various times for the TGDDM/DDS/BMI system during the degradation process. As already noted for the pure

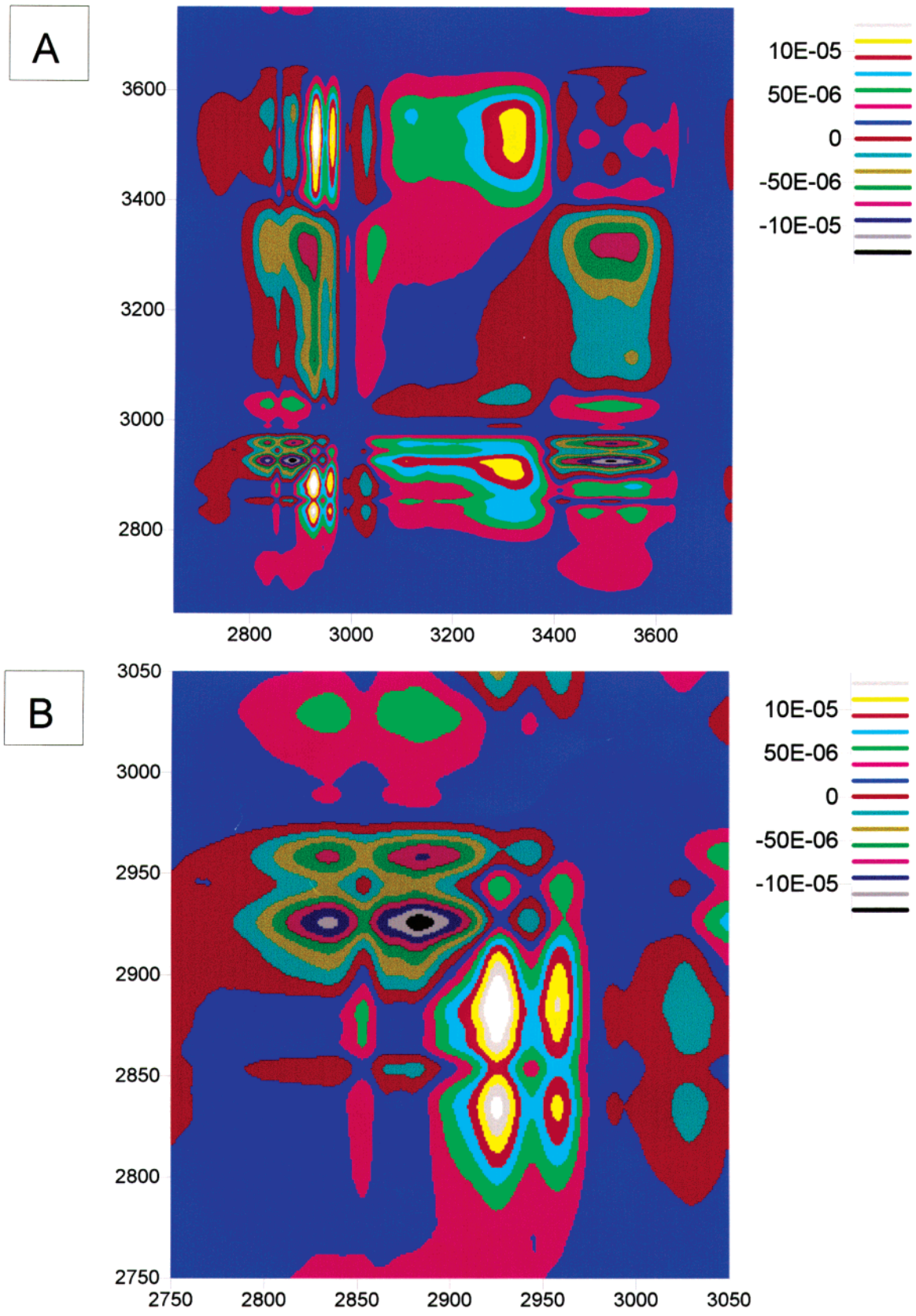

Figure 6. Asynchronous 2D correlation spectrum for the TGDDM/DDS network: (A) wavenumber range 2700−3800 cm^{-1}; (B) wavenumber range 2750−3050 cm^{-1}.

epoxy resin, the spectrum of the ternary system also changes substantially as a result of thermal oxidation. In particular, it is observed a steady increase of the carbonyl absorption along the wings of the principal component (the ν_{as} mode on of the imide carbonyl). The aromatic peaks centered at 1592 and 1510 cm^{-1} decrease in intensity, especially the latter. Clearly, due to the presence of the BMI component, the spectrum is more complex and less resolved than that of the parent network, and therefore, the application of bidimensional

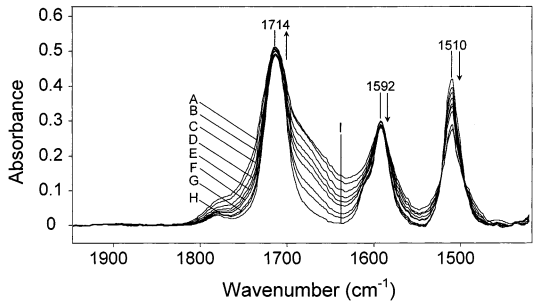

Figure 7. Transmission FTIR spectra in the wavenumber range 1950−1400 of the TGDDM/DDS/BMI network collected in situ at different times during thermal-oxidative degradation. Traces: (A) collection time, t, = 0 min; (B) t = 25 min; (C) t = 50 min; (D) t = 75 min; (E) t = 125 min; (F) t = 250 min; (G) t = 500 min; (H) t = 750 min; (I) t = 1000 min. The arrows' directions indicate absorbance increase or decrease of the corresponding peaks.

analysis is expected to be even more effective in this case.

Figure 8 shows the synchronous spectrum derived from the data of Figure 7. Three autopeaks can be distinguished at [1735, 1735 cm^{-1}], [1680, 1680 cm^{-1}], and [1510, 1510 cm^{-1}], whose correlation produce three corresponding cross-peaks at the relative frequency coordinates. The higher frequency autopeak is related to the imide carbonyl, while the remaining two autopeaks and the relative cross-peaks are coincident with those already observed and discussed for the case of the neat epoxy system.

In Figure 9 is reported the asynchronous spectrum in the 1420−1900 cm^{-1} range. A direct comparison with the corresponding spectrum of the epoxy system, evidences several interesting features. First of all, an exactly coincident pattern can be identified in the two correlation spectra, with respect to both the position and sign of the cross-peaks, comprising most of the features present in the pure epoxy resin. From the point of view of the thermal-oxidative mechanism, the above observation is very relevant. It is, in fact, a direct evidence of a common degradation mechanism taking place in the two systems. Recalling that the ternary TGDDM/DDS/BMI mixture displays an IPN like molecular structure comprising a TGDDM-DDS network and a BMI homonetwork, it is concluded that the former network undergoes thermal-oxidative degradation independently of the presence of the BMI component.

The identification of characteristic patterns offers an additional advantage of 2D IR spectroscopy in the analysis of multicomponent reacting systems. The occurrence of features of this type, analogous or coincident to those present in the 2D spectra of the parent systems, constitutes a sort of "molecular mechanism fingerprint" which positively identifies specific reaction pathways and indicates that the presence of the additional component(s) do not alter the original reaction mechanism but adds, if that be the case, additional, independent reaction pathways.

In the spectrum of Figure 8, additional cross-peaks are generated by correlation with a component at 1735 cm^{-1}, and appear at [1735, 1676 cm^{-1} (−)], [1735, 1591 cm^{-1} (−)], and [1735, 1500 cm^{-1} (−)]. The 1735 cm^{-1} feature, being absent in the binary mixture spectrum, is clearly related to the BMI carbonyl, and more specifically, to the ν_{as} mode originally centered at 1714 cm^{-1}. The fact that the frequency at which the cross-peaks appear is considerably higher than the original position of the carbonyl absorption is not easily accounted for. Tentatively, it might be ascribed to a gradual shift toward higher wavenumbers of the peak position, and/or to an interfering effect caused by the

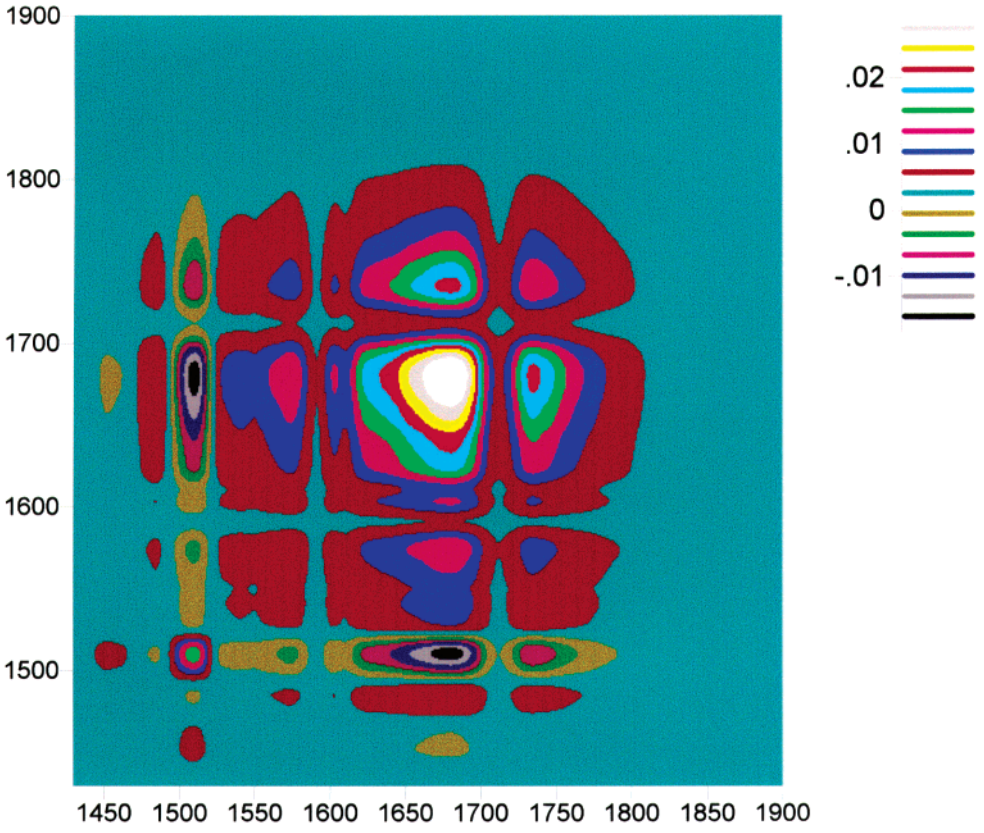

Figure 8. Synchronous 2D correlation spectrum in the wavenumber range 1450−1900 cm^{-1} for the TGDDM/DDS/BMI network.

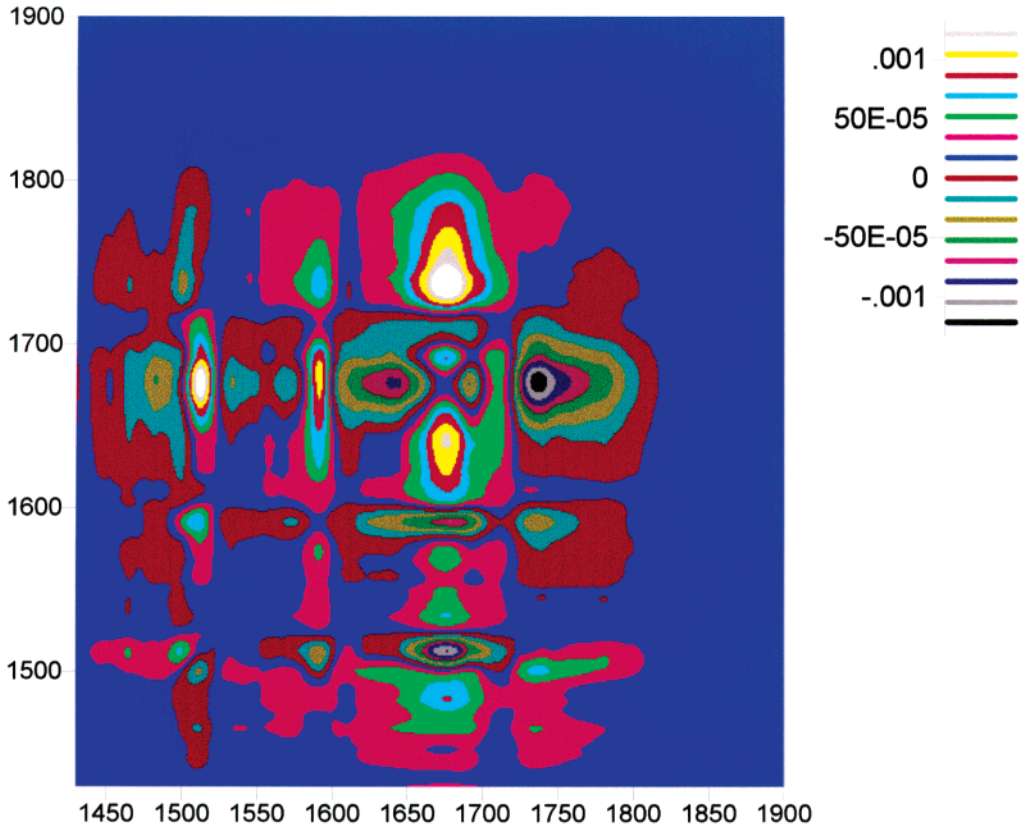

Figure 9. Asynchronous 2D correlation spectrum in the wavenumber range 1450 −1900 cm^{-1} for the TGDDM/DDS/BMI network.

contribution of the concurrently growing carbonyl groups arising from the oxidative degradation of the TGDDM/DDS network. In any event, the above features indicate the involvement of the BMI homonetwork in the degradation process; the sign of the cross-peaks evidence that the imide carbonyls decay at a slower rate than the oxygen-sensitive groups of the TGDDM/DDS network (CH, OH, TGDDM and DDS aromatic rings) and such a lower degradation rate of BMI represents the underlying reason for the enhanced temperature stability of the ternary system as compared to the binary TGDDM/DDS resin.

In the asynchronous spectrum of the TGDDM/DDS/BMI system it is noted a further cross-peak at [1510, 1500 cm^{-1} (−)] which is absent in the spectrum of the parent network. It originates from the cross-correlation of the TGDDM aromatic absorption located at 1510 cm^{-1} with the analogous vibrational mode of the BMI unit, which absorb at a slightly lower frequency, as revealed by the spectrum of the neat imide monomer. These two components are completely overlapped in the frequency spectrum, but are resolved in the 2D spectrum. The sign of the cross-peak confirms the already noted temporal relationship, i.e., that the degradation of the BMI network is slower than that of the TGDDM/DDS network.

2600—3800 cm^{-1} Range. The sequence of FTIR spectra for the ternary system in the wavenumber range 3800−2600 cm^{-1} is reported in Figure 10, while the synchronous spectrum calculated therefrom is shown in Figure 11. The latter resembles very closely that of the unmodified epoxy resin, the only relevant difference being the position of the high-frequency autopeak, which is found at [3540−3540 cm^{-1}], while the corresponding feature in the epoxy resin spectrum is located about 30 cm^{-1} below. This simply reflects the initial position of

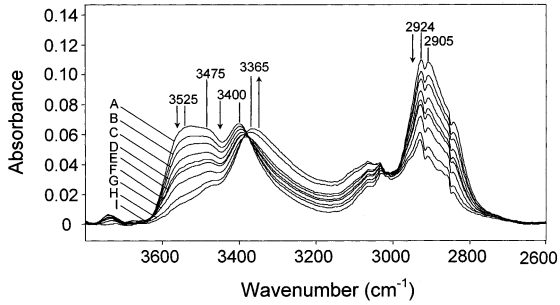

Figure 10. Transmission FTIR spectra in the wavenumber range 3800−2600 of the TGDDM/DDS/BMI network collected in situ at different times during thermal-oxidative degradation. Traces: (A) collection time, t, = 0 min; (B) t = 25 min; (C) t = 50 min; (D) t = 75 min; (E) t = 125 min; (F) t = 250 min; (G) t = 500 min; (H) t = 750 min; (I) t = 1000 min. The arrows' directions indicate absorbance increase or decrease of the corresponding peaks.

the broad ν_{OH} band giving rise to the autopeak, which, in the ternary network is displaced toward higher frequencies, as a consequence of a different distribution of hydrogen-bonding interactions in the two systems. The close correspondence of the synchronous spectra of the two investigated networks is to be expected owing to the predominance of the TGDDM/DDS spectrum over that of the BMI in the present frequency range. However, this result further confirms the occurrence of the same reaction mechanism in the two cases, involving selectively the TGDDM/DDS network.

The same conclusion can be drawn by inspection of the asynchronous spectrum of the TGDDM/DDS/BMI mixture (see Figure 12). Features analogous to those observed in the corresponding spectrum of the unmodified epoxy resin are found at [3542, 3330 cm^{-1} (−)], [3542, 3030 cm^{-1} (−)], [3325, 2915 cm^{-1} (+)], [3325, 2831

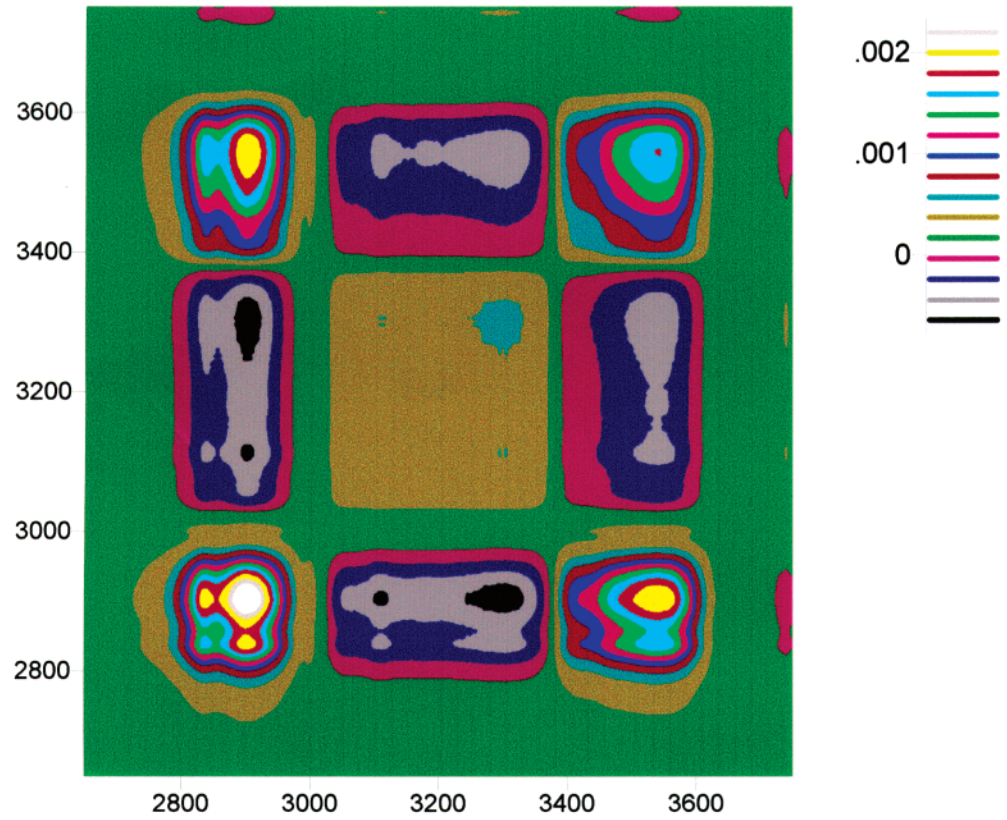

Figure 11. Synchronous 2D correlation spectrum in the wavenumber range 2700−3800 cm^{-1} for the TGDDM/DDS/BMI network.

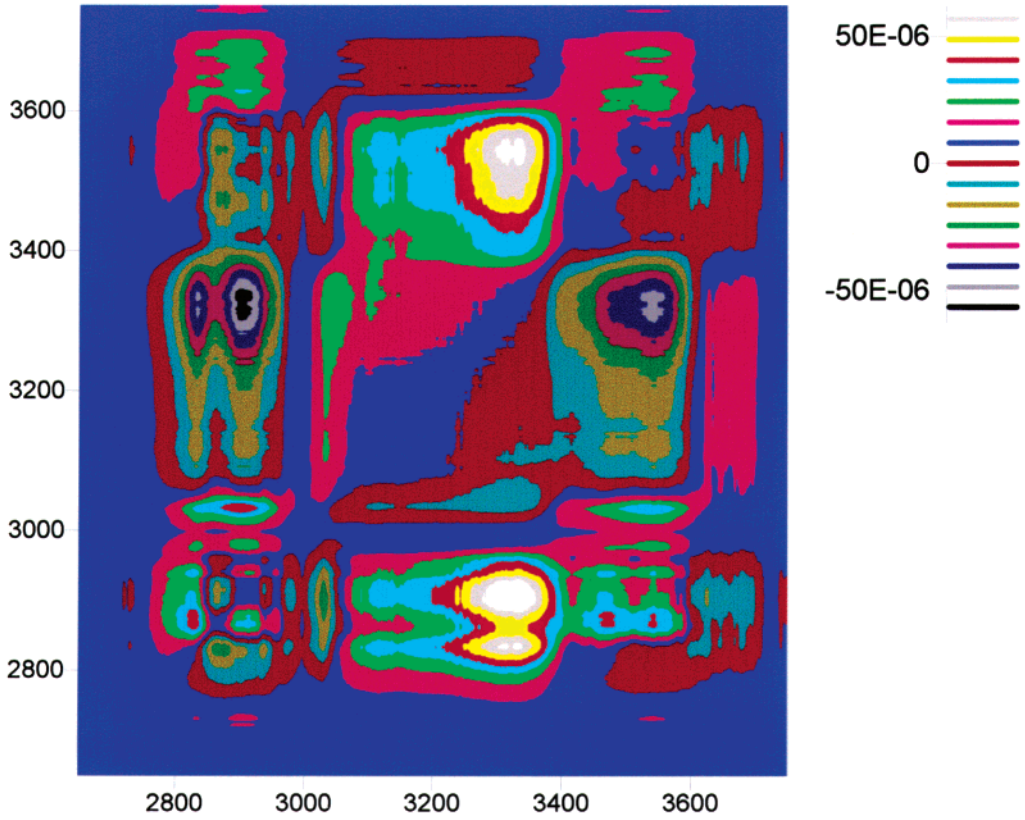

Figure 12. Asynchronous 2D correlation spectrum in the wavenumber range 2700−3800 cm^{-1} for the TGDDM/DDS/BMI network.

cm^{-1} (+)], and [3031, 2915 cm^{-1}] and can be analogously interpreted. In the aliphatic ν_{CH} range, the asynchronous spectrum is further complicated by the presence of components due to the CH_2 stretching of BMI, which contribute to worsen the resolution.

Concluding Remarks

The present contribution has demonstrated the usefulness of 2D IR analysis as an advanced interpretative tool for time-resolved FTIR data, in studies on high-

temperature, thermal-oxidative degradation of polymers. In particular, it has been shown that, for systems showing an exponentially decaying dynamic behavior, a considerable enhancement of resolution can be achieved by spreading the spectrum over the second frequency domain, especially in the case of the asynchronous cross-correlation spectrum, which, due to its peculiar functional form is more specific and richer of information.

The application of the bidimensional cross-correlation approach to analyze the degradation behavior of two TGDDM based systems, led to the following conclusions:

•The aliphatic chain of the TGDDM/DDS network is involved in the molecular breakdown process in its entirety, i.e., with the disappearance of hydroxyl, CH_2 and CH groups.

•The oxygen attack causes the formation of several oxygenated species, deriving from two concurrent and competitive pathways. One of these paths gives rise to the formation of amide groups, while the other leads to aldehyde and/or ketone functionalities. The mechanism producing amide groups seems to prevail over that leading to aldehyde/ketone groups.

•The auto-oxidation sequence gives rise to depletion of the disubstituted aromatic rings of both the TGDDM and DDS units. However, the decay in concentration of TGDDM aromatics is faster than that of DDS aromatics, and this result has been taken as an evidence of an alternative mechanism starting at the diphenyl-substituted methylene group of the TGDDM unit. Such a mechanism is found to be faster than that starting at the aliphatic chain, likely by dehydration, followed by allylic hydrogen abstraction.

•The ternary system comprising TGDDM, DDS, and BMI is found to produce cross-correlation spectra having similar patterns than those of the binary TGDDM/DDS network. This is an evidence that, in the IPN system, the TGDDM/DDS network degrades in exactly the same way as it does in the unmodified epoxy resin.

•The BMI homonetwork present in the IPN system is also found to undergo thermal-oxidative degradation. The degradative process involves the imide carbonyls, and the disubstituted aromatic rings. Some evidence of the involvement of the methylene group is also present in the asynchronous spectrum.

•In the IPN system the degradation rate of the BMI homonetwork is lower than that of the TGDDM/DDS network, and this represents the underlying reason for the enhanced stability of the ternary mixture as compared to the binary TGDDM/DDS system.

Acknowledgment. Thanks are due to Prof. L. Mascia and Dr. G. Ragosta for stimulating discussions and to Mr. G. Orefice for assistance in performing the FTIR measurements.

References and Notes

(1) May, C. A., Ed.; *Epoxy Resins, Chemistry and Technology*, 2nd ed.; Marcel Dekker Inc.: New York, 1988.
(2) Ellis, B., Ed. *Chemistry and Technology of Epoxy Resins*; Blackie Academic and Professional: Glasgow, Scotland, 1993.
(3) Halpin, J. P.; Pandolfini, P. P.; Bierman, P. J.; Kistenmaker, T. J.; Hunter, L. W.; O'Connor, J. S.; Jablonski, D. *APL Technol. Dig.* **1997**, *18*, 33.
(4) Domeier, L. A. US Pat. 4,654,407, 1987.
(5) Pigneri, A. M.; Galoci, E. C.; Jackson, R. J.; G. C. Young, *1st Int. SAMPE Electron. Conf.* **1987**, *1*, 657.
(6) Woo, E. M.; Chen, L. B.; Seferis, J. C. *J. Mater. Sci.* **1987**, *22*, 3665.
(7) Musto, P.; Martuscelli, E.; Ragosta, G.; Russo, P.; Scarinzi, G. *J. Appl. Polym. Sci.* **1998**, *69*, 1029.
(8) Musto, P.; Martuscelli, E.; Ragosta, G.; Russo, P.; Scarinzi, G.; Villano, P. *J. Mater. Sci.* **1998**, *33*, 4595.
(9) Musto, P.; Ragosta, G.; Russo, P.; Mascia, L. *Macromol. Chem. Phys.* **2001**, *202*, 3445.
(10) Noda, I. *Bull. Am. Phys. Soc.* **1986**, *31*, 520.
(11) Noda, I. *Bull. Am. Chem. Soc.* **1989**, *111*, 8116.
(12) Noda, I. *Appl. Spectrosc.* **1990**, *44*, 550.
(13) Noda, I. *Appl. Spectrosc.* **1993**, *47*, 1329.
(14) Noda, I.; Dowrey, A. E.; Marcott, C. *Appl. Spectrosc.* **1993**, *47*, 1317.
(15) Noda, I.; Dowrey, A. E.; Marcott, C.; Story, G. M.; Ozaki, Y. *Appl. Spectrosc.* **2000**, *54*, 236A.
(16) Ekgasit, S.; Ishida, H. *Appl. Spectrosc.* **1995**, *49*, 1243.
(17) Nakano, T.; Shimada, S.; Saitoh, R.; Noda, I. *Appl. Spectrosc.* **1993**, *47*, 1337.
(18) Elmore, D. L.; Dluhy, R. A. *Appl. Spectrosc.* **2000**, *54*, 956.
(19) Kimura, F.; Komatsu, M.; Kimura, T. *Appl. Spectrosc.* **2000**, *54*, 974.
(20) Ozaki, Y.; Liu, Y.; Noda, I. *Appl. Spectrosc.* **2000**, *54*, 526.
(21) Murayama, K.; Czarnik-Matusevicz, B.; Wu, Y.; Tsenkovaa, R.; Ozaki, Y. *Appl. Spectrosc.* **2000**, *54*, 978.
(22) Wu, P.; Yang, Y.; Siesler, H. W. *Polymer* **2001**, *42*, 1018.
(23) Nabet, A.; Auger, M.; Pezolet, M. *Appl. Spectrosc.* **2000**, *54*, 948.
(24) Noda, I. *Appl. Spectrosc.* **2000**, *54*, 994.
(25) Czarnecki, M. A. *Appl. Spectrosc.* **1998**, *52*, 1583.
(26) Czarnecki, M. A. *Appl. Spectrosc.* **1999**, *53*, 1392.
(27) Bellamy, L. J. *The Infrared Spectra of Complex Molecules*; Chapman and Hall: New York, 1975; Vols. 1−2.
(28) Colthup, N. B.; Daly, L. H.; Wiberley, S. E. *Introduction to Infrared and Raman Spectroscopy*; Academic Press: San Diego, CA, 1990.
(29) Roeges, N. P. G.; *A Guide to the Complete Interpretation of Infrared Spectra of Organic Structures*; Wiley: New York, 1994.

MA0214815